Applied Surface Science 470 (2019) 289–295

Contents lists available at ScienceDirect

Applied Surface Science

journal homepage: www.elsevier.com/locate/apsusc

Full Length Article

Oxidation resistance of a Mo-W-Si-B alloy at 1000–1300 °C: The effect of a multicomponent Mo-Si-B coating

Gaoyuan Ouyang[a,*], Pratik K. Ray[a], Srinivasa Thimmaiah[a], Matthew J. Kramer[a], Mufit Akinc[a], Patrick Ritt[b], John H. Perepezko[c]

[a] Department of Materials Science and Engineering and Ames Laboratory, US-Department of Energy, Iowa State University, Ames, IA 50011, USA
[b] ZYP Coatings, Inc., 120 Valley Court, Oak Ridge, TN 37830, USA
[c] Department of Materials Science and Engineering, University of Wisconsin – Madison, Madison, WI 53706, USA

ARTICLE INFO

Keywords:
Mo-Si-B
Coatings
Tungsten
Oxidation
Disilicides

ABSTRACT

The oxidation behavior and microstructures of a three phase $Mo_{50}W_{20}Si_{15}B_{15}$ alloy containing (Mo, W) solid solution, $(Mo, W)_5Si_3$ and $(Mo, W)_5SiB_2$ were investigated over the 1000–1300 °C temperature range. At 1300 °C, the alloy exhibited a large initial mass loss and eventually transitioned to a steady state behavior associated with the development of an amorphous borosilica scale. The oxidation resistance at lower temperature was unsatisfactory due to the pesting of Mo and W. Grazing Incident Angle X-ray Diffraction (GIXRD) measurements during the initial transient stage of oxidation identified the evolution of surface oxide products that were responsible for the large weight loss and pesting behavior. In order to address the large initial weight loss and the low temperature pesting behavior, the alloy was coated with a Mo-Si-B based coating by employing the pack cementation process followed by a conditioning treatment at 1450 °C. The microstructures of the coatings and the interlayer between the base alloy and the coating were studied, and the oxidation resistance of the coated alloys was evaluated over the 800–1300 °C temperature range. The coated alloy showed improved oxidation resistance with nearly zero mass change for extended period of time over the entire range of temperatures studied.

1. Introduction

Mo-Si-B alloys have long been considered as attractive candidates for high temperature applications [1–4]. Mo-rich alloys have exhibited reasonable strength and fracture toughness [5–7], while alloys rich in Si and B have shown excellent high temperature oxidation resistance [8–10]. The alloys studied by Berczik et al. [11,12] comprised of the metal rich solid solution, essential for providing toughness, existing in thermodynamic equilibrium with the T_2 (Mo_5SiB_2) phase and the A15 (Mo_3Si) phase showed promising mechanical properties.. The phase relationship in this region was studied by Nunes et al. [13]. The T_2 phase has excellent oxidation resistance due to a high metalloid content, resulting in the formation of a borosilicate scale that forms an excellent oxygen barrier [1,14]. The A15 phase, on the other hand, has very poor oxidation resistance [14]. Additionally, the A15 Mo_3Si intermetallic is extremely brittle due to the presence of only four active slip planes [15]. Alloys studied by Akinc et al. [8–10,16], on the other hand, were drawn from a ternary phase field comprising of the A15 phase, the T_2 phase and the T_1 (Mo_5Si_3) phase. The T_1 phase exhibited excellent creep resistance [17]; moreover, when saturated with B, the T_1 phase also demonstrated reasonable oxidation resistance [17]. However, the presence of intermetallics, especially the A15 phase (and the corresponding absence of the Mo rich solid solution) results in poor fracture toughness. The A15 phase can be destabilized by a number of alloying additions including Nb, Ta, W, Ti, Zr and Hf [18]. Addition of Ti to Mo-Si-B alloys is known to improve creep resistance [19]. However, the oxidation resistance of Ti substituted Mo-Si-B alloys is inadequate due to the formation of a duplex scale [20]. Recent work on application Mo-Si-B coating to the Mo-Si-B-Ti alloys has resulted in improved oxidation resistance [21]. Tungsten, though heavier in the atomic weight, effectively destabilized A15 phase with only 7–10 atomic percent required (critical Ti content for destabilizing the A15 phase is ~27.5at.%) [22,23]. W substituted Mo-Si-B also exhibits an improved oxidation resistance compared to Ti or Nb substituted Mo-Si-B, where a steady oxidation stage is displayed for Mo-W-Si-B after the initial mass loss [19]. The destabilization of A15 phase by W addition opens up a three phase region comprising of a metal rich solid solution that provides toughness, the T_2 phase that provides oxidation resistance

* Corresponding author.
E-mail address: gaoyuan@iastate.edu (G. Ouyang).

https://doi.org/10.1016/j.apsusc.2018.11.167
Received 19 July 2018; Received in revised form 6 November 2018; Accepted 20 November 2018
Available online 22 November 2018
0169-4332/

and the T_1 phase that provides creep resistance. However, the deterioration of oxidation resistance at lower temperatures (under 1300 °C) of Mo-W-Si-B alloys needs to be addressed.

An alternative approach to combining the toughness of metal rich alloys with the oxidation resistance of the intermetallic rich alloys would involve the application of a Mo-Si-B coating on the metal rich alloys. The coating is often applied by physical (PVD) or chemical vapor deposition (CVD) techniques. For PVD, several micron thickness of Mo_5Si_3, $MoSi_2$, MoB or $MoSi_2$, MoB mixture can be deposited by magnetron sputtering on the surface. For CVD, Si and B were applied by co-pack cementation, where Si and B were transported and diffused to the substrate as gaseous form activated by halide activator. Following the deposition, the samples undergone high temperature (as high as 1500 °C) conditioning to form an additional protective borosilicate outer layer. Recently, CVD coatings were shown to significantly prolong the lifetime of Mo-Si-B at 1300 °C oxidative environment [24]. There are also other reports on the oxidation performance improvements resulting from the application of silicide coatings to Mo-base and other refractory metal alloys [25–38]. In this paper, we study the oxidation behavior of a coated and uncoated Mo-W-Si-B alloy.

2. Material and methods

The alloys were prepared from elemental pieces of metals (Mo, W, Si and B) with 99.8% or higher purity (MPC, Ames, IA) by arc-melting elemental pieces on a water cooled copper hearth in an ultra-high purity argon atmosphere using a tri-arc melting unit. The nominal composition for the alloy is Mo (50 at.%), W (20 at.%), Si (15 at.%) and B (15 at.%). The arc-melted buttons were re-melted thrice in order to obtain a better homogeneity. These alloys were then drop-cast to yield cylindrical rods of approximately 10 mm diameter. These rods were then annealed in a tungsten mesh resistance furnace (M60, Centorr and associates inc., Nashua, NH) at 1850 °C for 10 h in order to further homogenize the samples. Several coupons were sectioned using electrical discharge machining. A Mo-Si-B coating was applied for some of these coupons, whereas the other coupons were oxidized without a coating.

The coatings were applied by pack cementation method. Before coating, samples were surface grounded using SiC paper up to 2500 grit. Samples were embedded into power pack mixture in an alumina crucible, where the mixture consisted of 34.03 wt% Si (99.95% purity, 45 µm, Alfa Aesar), 0.97 wt% B (99.95% purity, 45 µm, Alfa Aesar), 2.5 wt% NaF activator (Alfa Aesar), and 62.5 wt% Al_2O_3 spacer (180 µm). The alumina crucible was placed into an alumina tube which was sealed following evacuation of air and backfilled with Ar gas. The pack cementation was done at 1000 °C for 50 h in mild Ar flow. After pack cementation, the samples were conditioned at 1450 °C for 8 h in air to encourage to formation of outer borosilicate layer.

The cyclic oxidation experiments were carried out in a Lindberg Blue horizontal tube furnace using ambient air at the desired temperatures (800–1300 °C) for desired time intervals. Each cycle consisted of oxidation at the target temperatures for 60 min followed by an exposure to ambient temperature for 30 min. All the mass measurements were performed ex-situ after the samples had cooled down. No oxide scale spallation could be seen during this process. Alumina boats were used for containing the coupons. No reaction was observed with the alumina boats and the coupons. The isothermal oxidation studies were carried out at 800 °C and 1000 °C for 25 h using thermogravimetric analyzer (TGA, Cahn, TG-131) with flowing ultra-high purity synthetic air (20% O_2, 80% N_2) at a flow rate of 50 mL/min. Phase analysis of the alloy and the oxidized coupon was carried out by X-ray diffraction (XRD) using Bragg-Brentano geometry with a Philips PANalytical X-ray diffractometer equipped with a double-bent monochromator and a copper target. The Grazing Incidence angle X-ray diffraction (GIXRD) was carried out using Bruker DaVinci D8 system using 1°incident angle. Microstructural analysis of the alloys as well as the oxidized coupons was carried out using a JEOL 5910Lv Scanning Electron Microscope (SEM). The phase compositions were investigated using wavelength dispersive spectroscopy (WDS).

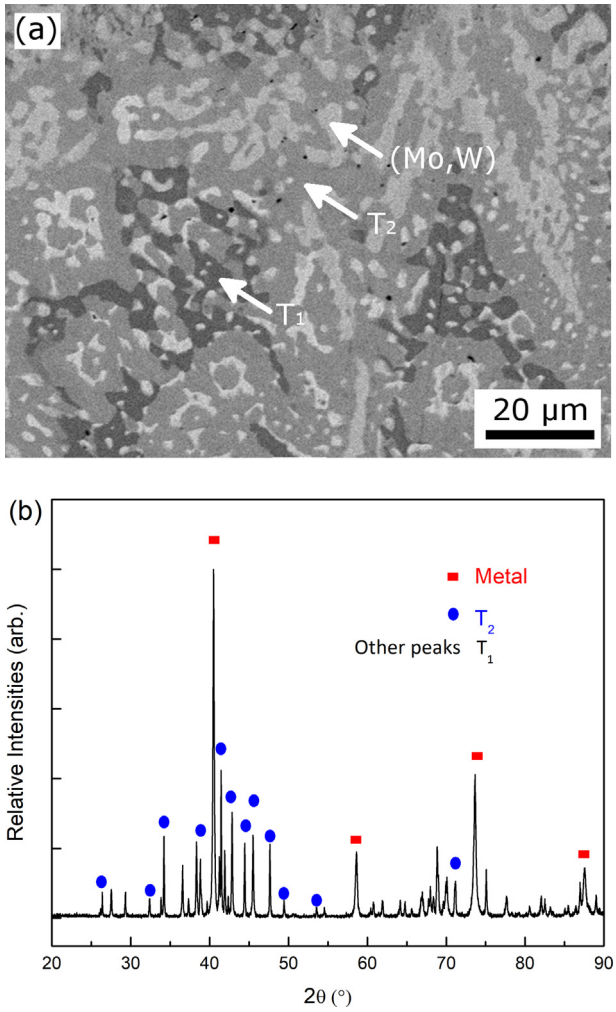

Fig. 1. (a) Microstructure of the base alloy; (b) X-ray diffractogram from the base alloy – the unlabelled peaks indicate the T_1 phase.

3. Results and discussion

Fig. 1(a) shows the microstructure of the base alloy. The base alloy has a three phase microstructure comprising of a metal rich (Mo, W) solid solution, a T_1 (Mo, W)$_5Si_3$ phase and a T_2 (Mo, W)$_5SiB_2$ phase. The A15 Mo_3Si phase was not observed in the microstructure. The presence of these three phases (as well as the absence of the A15 phase) is further confirmed by the X-ray diffraction pattern from the base alloy, shown in Fig. 1(b). The diffraction pattern did not show any noticeable peak shifts, which is not surprising considering that Mo and W have very similar atomic radii [39]. EDS analyses indicated the solid solution to consist of approximately 55 atom% Mo and 45 atom% W. A precise quantification of the W content in the T_1 and T_2 phases could not be obtained using the EDS due to a significant overlap of the W M_α line and the Si K_α lines (1.77 keV vs 1.74 keV). However, based on the W L_α peak (8.39 keV) it is apparent that the T_2 phase had a higher W content than the T_1 phase. This becomes further apparent from the Z contrast observed in the back-scattered electron mode (T_2 shows up brighter in comparison to T_1 despite having larger boron content). The partitioning of W can be understood from a thermodynamic perspective, using Miedema's model and *ab-initio* studies available in the literature [22,40–42]. The Mo-Si interactions are stronger in comparison to W-Si

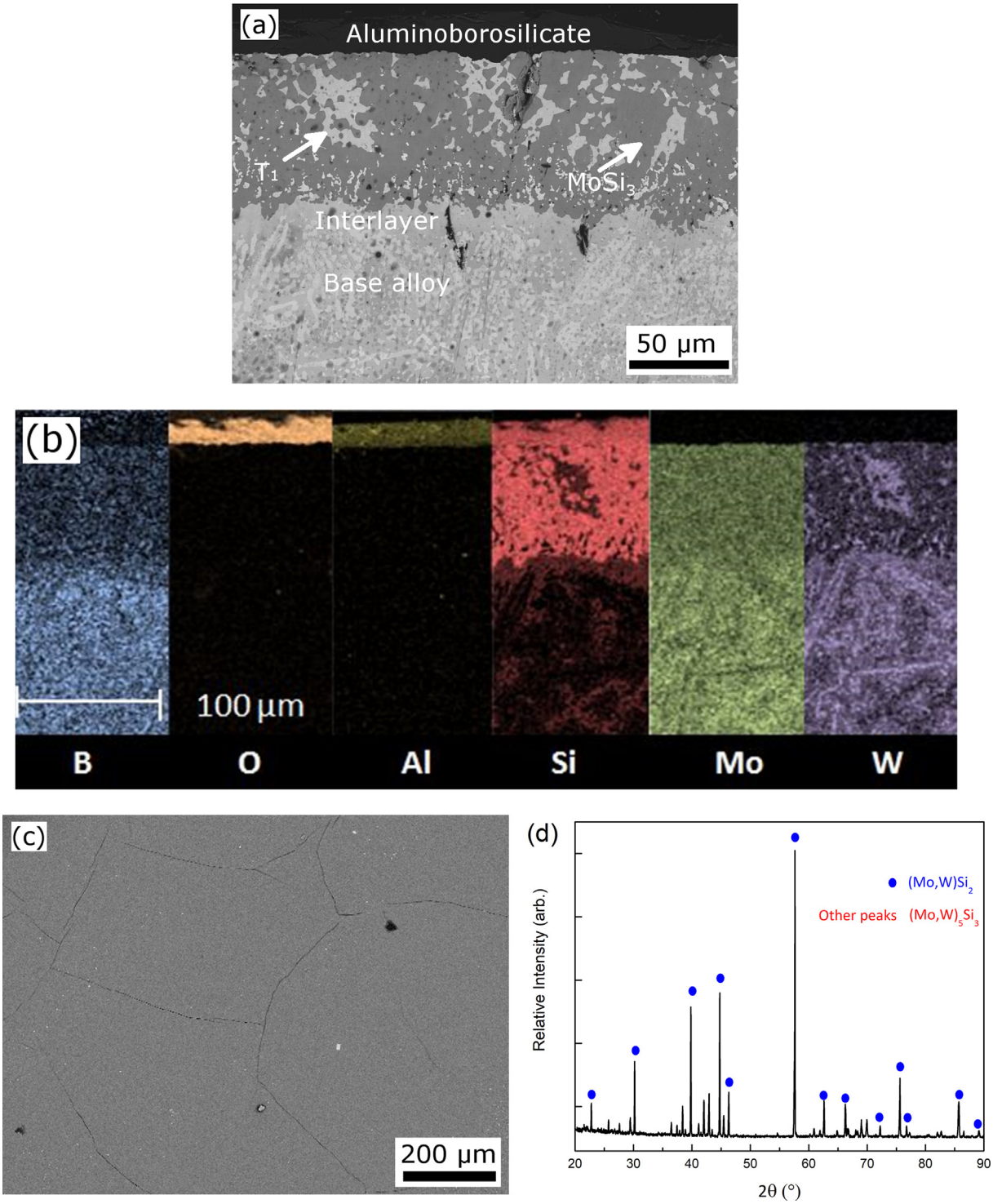

Fig. 2. (a) Cross-section microstructures of the coated alloy; (b) EDS elemental map of the coated alloy – each slice represents the distribution of a given element from the same region of the microstructure; (c) Surface micrograph of the coated alloy; (d) X-ray diffractogram from the coated surface – the unlabelled peaks indicate the T_1 (Mo, W)$_5$Si$_3$ phase.

interactions [41,42]. This is, for instance, reflected in the change in formation enthalpies, with the enthalpy values becoming less negative, with increasing W addition to silicides such as the A15 phase [22]. The thermodynamics of borides of tungsten and molybdenum have been studied extensively theoretically and experimentally [43,44], and the formation enthalpies of Molybdenum borides and tungsten borides are similar. Consequently, the partitioning is driven by maximizing Mo-Si bonds at the expense of W-Si bonds. Hence, the W is preferentially "driven" into the metal rich solid solution. The larger number of M—Si bonds (M = metal) in M_5Si_3, in comparison to M_5SiB_2 also results in preferential partitioning of W to the M_5SiB_2 T_2 phase as opposed to the M_5Si_3 T_1 phase [45]. Consequently, the T_2 phase is expected to have a higher W content in comparison to the T_1 phase (although not as high as the metal rich solid solution). This is, in fact, reflected by the Z contrast in the backscattered SEM images, where the T_2 phase containing B shows a brighter contrast in comparison to the T_1 phase.

Fig. 2(a) shows the cross-section microstructure of the coated Mo-W-Si-B alloy. The microstructure comprises of three major regions – a thin oxide layer at the top, followed by the Mo-Si-B coating, an interlayer between the coating and the base alloy, and the base alloy itself. Fig. 2(b) shows the EDS elemental map collected from the corresponding region. The elemental map shows the presence of aluminum, silicon, oxygen and a small amount of boron in the top layer, indicating this to be the aluminoborosilicate layer. This aluminoborosilicate layer was also observed by other researchers [24], which originates from the Al that is incorporated from the pack powder. The second layer in the Mo-Si-B coating structure is comprised of (Mo, W)Si_2 and T_1 (Mo, W)$_5Si_3$. The presence of the (Mo, W)Si_2 is in agreement with the results reported by Lu-Steffes et al. [46] following the pack cementation of pure W with Mo-Si-B. Underneath the coating, a T_1 (Mo, W)$_5Si_3$ interlayer was observed to form as well. The tungsten content in the base alloy seems to be higher in comparison to the coating since the interdiffusion between Mo and W is extremely sluggish [47]. Fig. 2(c) shows the surface microstructure of the coated alloy. In general, it can be seen that the coating provides a good overall surface coverage. However, minor cracks could still be observed. Fig. 2(d) shows the X-ray diffraction pattern collected from the coating surface. It can be seen clearly that the major phases visible are the C11b (Mo, W)Si_2 and the T_1 (Mo, W)$_5Si_3$. This is in complete agreement with the SEM micrographs and EDS analyses presented in Fig. 2(a) and (b).

The uncoated sample, following oxidation at 1200 and 1300 °C, showed a change in appearance due to the formation of a glassy oxide scale. When oxidized at lower temperatures, i.e., 1000 °C and 1100 °C, the samples disintegrated as a consequence of pesting. The coated samples, on the other hand, showed no discernable changes after oxidation at 800–1300 °C. The cyclic oxidation kinetics of the coated and uncoated alloys are shown in Fig. 3(a). The coated alloys showed negligible mass change over the full range of temperature studied under cyclic conditions as shown in Fig. 3(a). Additional cyclic tests of the coated alloys up to 25 h from 800 °C to 1300 °C further confirm the relatively long term oxidation stability of the coated alloys as shown Fig. 3(b). The difference in mass change, as seen in Fig. 3(b) over an extended period of time is rather negligible, which becomes obvious when compared with Fig. 3(a). The uncoated alloys lose significant mass at lower temperatures, i.e. at 1000 and 1100 °C. However, this alloy appears to approach a steady state oxidation behavior at 1200 and 1300 °C. Moreover, based upon previous work [19] there is a trend towards an increase in the mass loss upon approach to steady state with increasing W addition as well as the expected increase with increasing exposure temperature. A quantitative comparison is difficult since the steady state mass loss level is a function of individual phase size as well as composition [14]. These results appear to mirror the work of Yoon et al. [48]. They observed that the oxidation resistance of WSi_2 deteriorates as the temperature was increased to 1200 °C. However, a further increase in temperature to 1300 °C resulted in a lower mass change. This apparent improvement in oxidation behavior at 1300 °C was attributed to the rapid formation of an exclusive SiO_2, with the $(WO_3)_3$ steadily volatilizing. The presence of boron in the alloy under investigation is likely to change the kinetics of oxide scale development, due to the formation of a glassy borosilicate layer, which covers the surface of the alloy. Boron modifies the viscosity of the glassy oxide scale, and therefore provides more rapid surface coverage in comparison to a pure silica scale [1]. Yoon et al. attributed the rapid oxidation behavior of WSi_2 at 1200 °C to the formation of cracks and pores during the pesting of W, which resulted in numerous short-circuit diffusion pathways for the oxygen. The presence of the glassy borosilicate scale allows the cracks and pores in the surface to get covered faster. The mass changes in the coated alloys are negligible compared to the uncoated alloys and as reported in other work the negligible mass change continues for longer times (> 100 h) [49]. More importantly, the Mo-Si-B coating appears to have improved oxidation resistance at the lower temperatures (800 °C and 1000 °C) and is therefore able to suitably

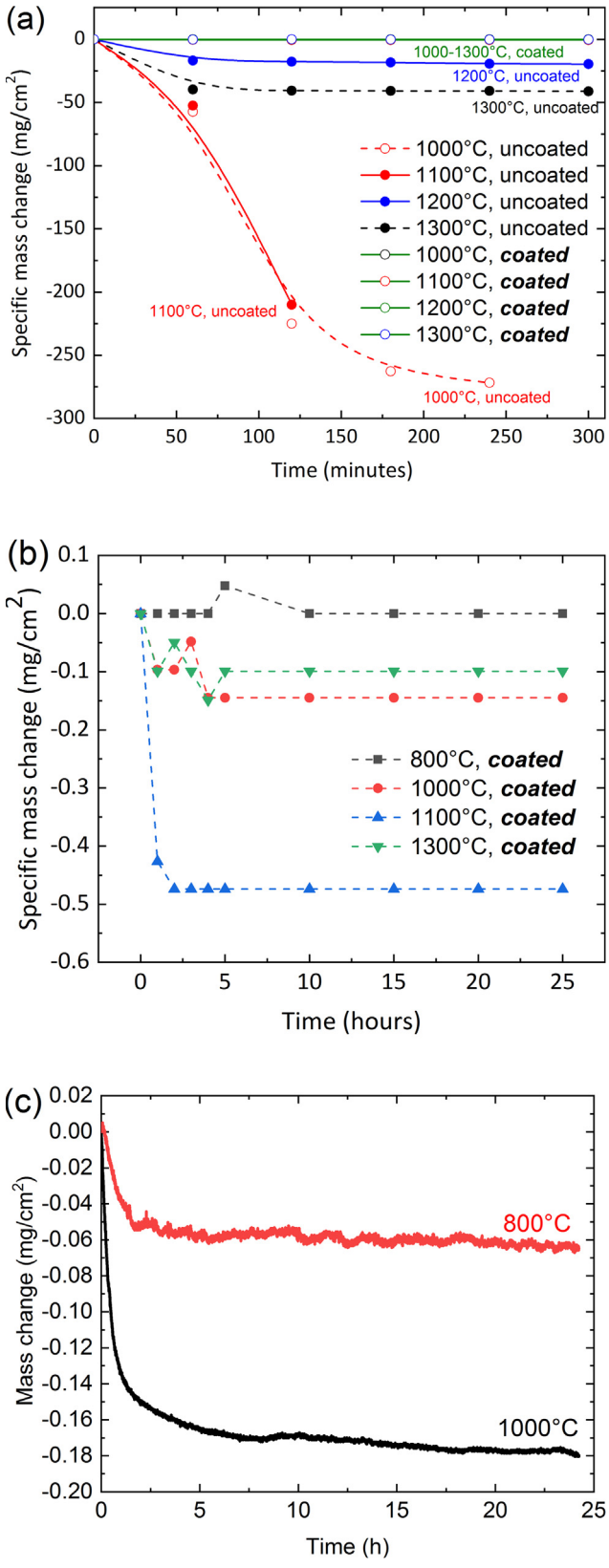

Fig. 3. (a) Cyclic oxidation kinetics of the coated and uncoated alloy between 1000 and 1300 °C for a total of 5 h; (b) Extended cyclic oxidation kinetics of the coated alloys between 800° and 1300 °C for 25 h; (c) isothermal oxidation kinetics of the coated alloy at 800 °C and 1000 °C.

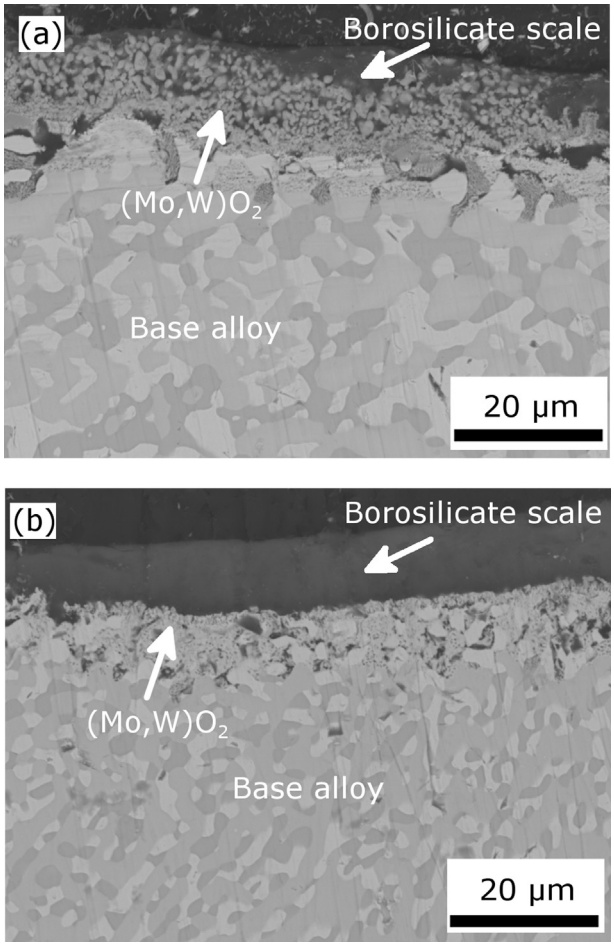

Fig. 4. Cross-section microstructures of the uncoated alloy at (a) 1200 °C and (b) 1300 °C.

protect the underlying base alloy. Fig. 3(c) shows the isothermal oxidation kinetics of the coated alloy at 800 °C and 1000 °C for 25 h. Following a minor initial mass loss, no significant mass change could be observed as a function of time. Therefore, it is evident that the coating affords improved oxidation protection at temperatures in the pesting range, even over extended periods of time.

Fig. 4(a) and (b) shows cross-section microstructures of the uncoated alloy at 1200 °C and 1300 °C respectively. A glassy borosilicate oxide layer forms on the surface at both temperatures, with the alloy oxidized at 1300 °C exhibiting a thicker borosilicate scale. The amount of WO_x entrapped in the oxide scale is significantly larger at 1200 °C as opposed to 1300 °C. The scale formed is non-planar in nature, due to the discontinuous presence of the metal-rich phase. The metal-rich solid solution phase oxidizes more rapidly in comparison to the T_1 and T_2 phase. However, once the borosilicate scale forms, a lower oxygen partial pressure in the subscale region at the oxide/alloy interface results in the formation of (Mo, W)O_2, forming finger-like incursions in the alloy. While the vapor pressure of $(MoO_3)_3$ starts increasing sharply as a function of temperature around 700 °C, the vapor pressures of $(WO_3)_3$ shows a qualitatively similar increase at temperatures approaching 1300 °C [46]. Consequently a greater amount of the oxides of W remain entrapped in the borosilicate scale at 1200 °C as compared to 1300 °C. These results bear some parallel to the oxidation studies on pure W coated with Si + B by Lu-Steffes et al. [46]. They observed the formation of an aluminoborosilica layer (alumina being present as a consequence of the pack-cementation process involving inert alumina filler), with a significant amount of WO_3 remaining entrapped in the scale. The uncoated alloy presents a virgin surface containing all four

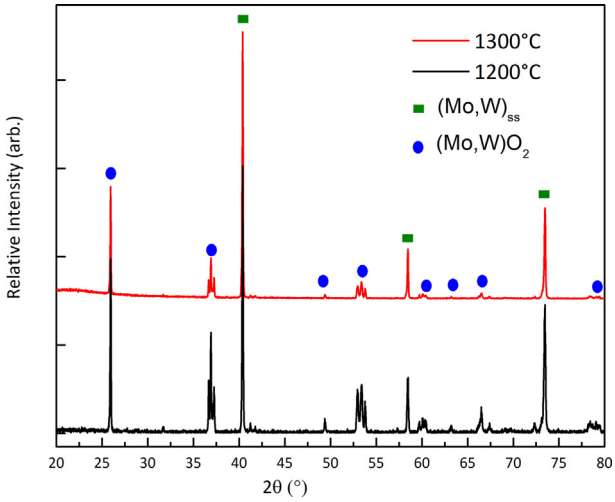

Fig. 5. X-ray diffraction patterns collected from the surfaces of the uncoated alloys oxidized at 1200 and 1300 °C for 5 h.

elements Mo, W, Si and B in terms of (Mo, W) solid solution, T_1 (Mo, W)$_5Si_3$ and T_2 (Mo, W)$_5SiB_2$. Mo oxidizes to form MoO_3, which rapidly volatilizes as $(MoO_3)_3$ at the temperatures being studied. The rate of evaporation of $(WO_3)_3$ is much slower in comparison to $(MoO_3)_3$; hence a significant amount of WO_x stays entrapped in the oxide scale. The presence of boron and silicon results in the formation of a low viscosity borosilicate layer that results in a faster surface coverage (in comparison to pure SiO_2). At temperatures of 1100 °C and below, the growth rates of the borosilicate scale is rather slow [48], and the silicon and boron content too low for complete surface coverage. Hence, a significantly larger mass change occurs, as the alloy coupons pest completely. Therefore, it is inferred that lower temperatures ($T < 1200$ °C) represent the more severe oxidative conditions for this alloy. Fig. 5 shows the X-ray diffraction patterns collected from the surface of the oxide scale after 5 h of oxidation. The diffraction patterns show a small hump around $2\theta = 20^\circ$, which is due to the formation of a glassy borosilicate scale. In addition to this, the metal peaks can be seen clearly. Furthermore, peaks ascribed to (Mo, W)O_2 show up as well. The formation of a borosilicate scale results in a drop in the oxygen partial pressure in the subscale region. The low oxygen partial pressure results in the formation of the metal dioxide instead of the trioxide.

GIXRD measurements were carried out during the transient oxidation stage of the MoWSiB alloys in order to ascertain the evolution of the surface oxide scale. A detailed analysis of the GIXRD data has been presented in the Supplementary section. Here, we present a synopsis of the results which highlights the transient oxidation pathways and temperature dependent mechanistic changes during initial stages of oxidation at 1100 and 1300 °C. Fig. 6(a) shows the GIXRD pattern as a function of oxidation time at 1100 °C. The unoxidized sample shows a combination of the metal-rich solid solution, T_1 and T_2 phase. With increasing oxidation time, the metal and intermetallic peaks reduce in intensity, with a corresponding appearance of the WO_3 peaks. The (Mo, W)O_2 is nearly absent in all the GIXRD data for samples oxidized at 1100 °C. MoO_3 is absent at the surface due to rapid evaporation above 700 °C [19]. After 2 min of oxidation, it can be seen that we have obtained a significant oxide scale coverage and thickness, with the peaks from the underlying solid solution and intermetallic phases being completely absent. Therefore, at 1100 °C, surface oxidation proceeds with the formation of WO_3 (in addition to the borosilicate scale, which can be seen in Fig. 4), and this oxide persists at the surface. An overall mass loss is still expected however, due to the volatilization of MoO_3 as the $(MoO_3)_3$ trimer [19]. The presence of WO_3 in the oxide scale results in a discontinuous surface coverage by the borosilicate scale, resulting in continued MoO_3 evaporation resulting in a monotonic mass loss

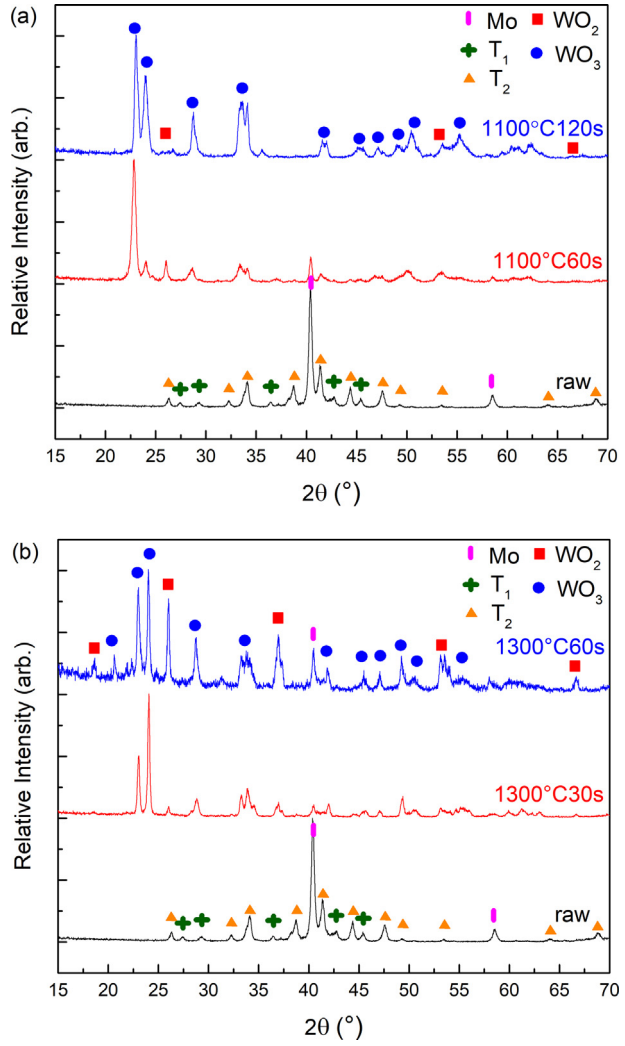

Fig. 6. Grazing incident angle X-ray diffraction (GIXRD) patterns collected from the surfaces of the uncoated alloys oxidized at (a) 1100° and (b) 1300 °C during the transient oxidation stage.

during the oxidation process. In contrast, the alloy exhibits a different oxidation mechanism when oxidized at 1300 °C, as evident from the GIXRD data shown in Fig. 6(b). While the intensity of the metal-rich solid solution and the intermetallics decrease, indicating a reasonable depth and coverage of the oxide scale at the surface, with a corresponding increase in intensity of the WO_3 peaks, the (Mo, W)O_2 appears as well after 60 s of oxidation. Coupled with the oxidized cross-section micrographs shown in Fig. 4 and the XRD pattern in Fig. 5, this indicates that WO_3 does form initially, and then volatilizes after longer exposures, with the subsurface (Mo, W) being further oxidized to (Mo, W)O_2. The loss of WO_3 results in uninterrupted surface coverage by the borosilicate scale, resulting in improved oxidation at 1300 °C in comparison to 1100 °C.

Fig. 7(a) and (b) shows the cross-section microstructures of the coated alloys at 1000 °C and 1300 °C for 25 h and 5 h respectively. It can be seen that there is very little change in the oxide scale as opposed to the un-oxidized sample. The aluminoborosilicate scale formed during the pre-treatment of the coating provides an excellent oxygen barrier. The absence of MoO_2 or WO_2 further indicates the efficacy of the Mo-Si-B coating. The coating, however, does indicate the presence of a number of cracks, which form during cooling due to the difference in thermal expansion coefficients between the disilicide and the T_1 phase in the coating [50] and stop at the T_2 phase. The insets in Fig. 7(a) and (b) show high magnification SEM micrographs of the cracked region. It

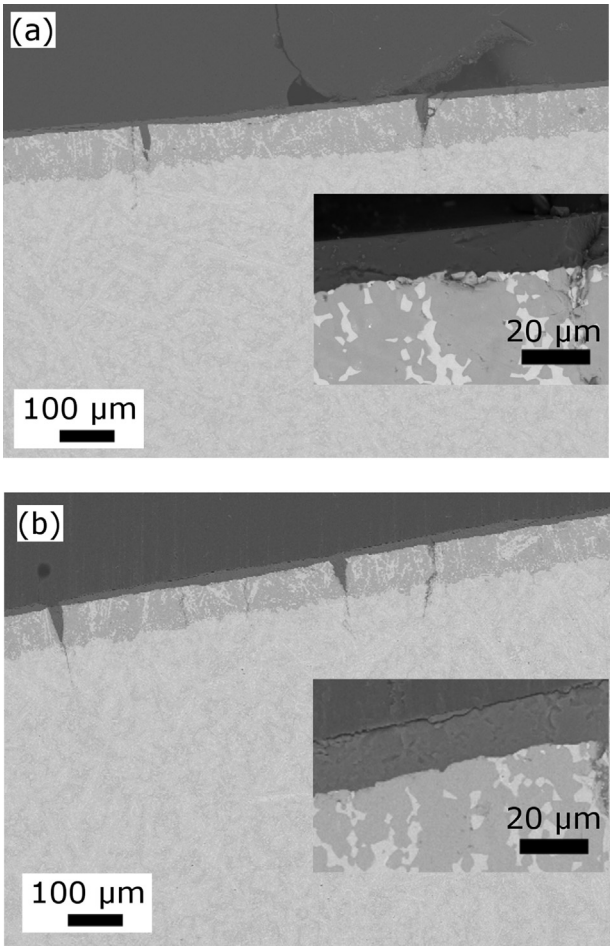

Fig. 7. Cross-section micrographs of the coated alloy after oxidation at (a) 1000° and (b) 1300 °C.

can be seen that this region comprises of the glassy oxide scale. If these cracks are limited to the coatings, then the self-healing nature of the coating serves to "heal" these cracks, thereby protecting the underlying base alloy from oxidation. The oxidation behavior of the coated alloys, therefore, shows a significant improvement in comparison to materials like WSi_2 [48] as well as the uncoated alloy.

4. Conclusions

The oxidation behavior of a $Mo_{50}W_{20}Si_{15}B_{15}$ alloy was studied over a range of temperatures, between 1000 and 1300 °C. It was seen that the alloy has superior oxidation resistance at higher temperatures compared to lower temperatures. GIXRD measurements confirmed that in the uncoated alloy the large initial weight loss during exposure at 1100 °C was related to the presence of WO_3 that disrupts the borosilica layer, but at 1300 °C the replacement of WO_3 by WO_2 yielded a continuous borosilica layer and improved performance. This was attributed to pesting oxidation of Mo and W at lower temperatures, combined with a relatively slower growth of the borosilicate scale. The performance of the alloy was improved significantly by applying a Mo-Si-B coating. The coated alloy was pre-treated at 1450 °C for 8 h. The top layer comprised of an aluminoborosilicate scale; the bulk of the coating, underneath the top layer comprised of (Mo, W)Si_2 and (Mo, W)$_5Si_3$. The coated alloys showed nearly none oxidation damages during both isothermal and cyclic oxidation tests from 800 °C to 1300 °C up to 25 h including the pesting temperatures. Clearly, the oxidation behavior of the coated alloy was significantly superior to the oxidation behavior of the uncoated Mo-W-Si-B alloy.

Acknowledgement

This work was supported by the AFOSR HTAM under contract # FA9550-11-1-201 and FA9550-17-1-0057 (JHP). We also thank M. Taylor, for his help with some of the coatings.

Appendix A. Supplementary material

Supplementary data to this article can be found online at https://doi.org/10.1016/j.apsusc.2018.11.167.

References

[1] M. Meyer, M. Kramer, M. Akinc, Boron-doped molybdenum silicides, Adv. Mater. 8 (1) (1996) 85–88.
[2] D.M. Dimiduk, J.H. Perepezko, Mo-Si-B alloys: developing a revolutionary turbine-engine material, MRS Bull. 28 (09) (2003) 639–645.
[3] J.A. Lemberg, R.O. Ritchie, Mo-Si-B alloys for ultrahigh-temperature structural applications, Adv. Mater. 24 (26) (2012) 3445–3480.
[4] M. Akinc, M.K. Meyer, M.J. Kramer, A.J. Thom, J.J. Huebsch, B. Cook, Boron-doped molybdenum silicides for structural applications, Mater. Sci. Eng., A 261 (1–2) (1999) 16–23.
[5] J.H. Schneibel, M.J. Kramer, D.S. Easton, A Mo–Si–B intermetallic alloy with a continuous α-Mo matrix, Scripta Mater. 46 (3) (2002) 217–221.
[6] J.H. Schneibel, P.F. Tortorelli, R.O. Ritchie, J.J. Kruzic, Optimization of Mo-Si-B intermetallic alloys, Metall. Mater. Trans. A 36 (3) (2005) 525–531.
[7] J.J. Kruzic, J.H. Schneibel, R.O. Ritchie, Fracture and fatigue resistance of Mo–Si–B alloys for ultrahigh-temperature structural applications, Scripta Mater. 50 (4) (2004) 459–464.
[8] M.K. Meyer, A.J. Thom, M. Akinc, Oxide scale formation and isothermal oxidation behavior of Mo–Si–B intermetallics at 600–1000 °C, Intermetallics 7 (2) (1999) 153–162.
[9] A.J. Thom, E. Summers, M. Akinc, Oxidation behavior of extruded Mo5Si3Bx–MoSi2–MoB intermetallics from 600°–1600 °C, Intermetallics 10 (6) (2002) 555–570.
[10] M.K. Meyer, M. Akinc, Isothermal oxidation behavior of Mo-Si-B intermetallics at 1450 °C, J. Am. Ceram. Soc. 79 (10) (1996) 2763–2766.
[11] D.M. Berczik, Comprising boron, silicon and metal described by a ternary system phase diagram; high strength; chemical resistance; jet engine parts, Google Patents, 1997.
[12] D.M. Berczik, Method for enhancing the oxidation resistance of a molybdenum alloy, and a method of making a molybdenum alloy, Google Patents, 1997.
[13] C.A. Nunes, R. Sakidja, Z. Dong, J.H. Perepezko, Liquidus projection for the Mo-rich portion of the Mo–Si–B ternary system, Intermetallics 8 (4) (2000) 327–337.
[14] F.A. Rioult, S.D. Imhoff, R. Sakidja, J.H. Perepezko, Transient oxidation of Mo–Si–B alloys: effect of the microstructure size scale, Acta Mater. 57 (15) (2009) 4600–4613.
[15] I. Rosales, J. Schneibel, L. Heatherly, J. Horton, L. Martinez, B. Campillo, High temperature deformation of A15 Mo 3 Si single crystals, Scripta Mater. 48 (2) (2003) 185–190.
[16] G. Ouyang, P.K. Ray, M.J. Kramer, M. Akinc, Pressureless sintering of Mo-Si-B alloys with Fe additive, J. Mater. Eng. Perform. 26 (5) (2017) 2417–2422.
[17] M.K. Meyer, M. Akinc, Oxidation behavior of boron-modified Mo5Si3 at 800°–1300°C, J. Am. Ceram. Soc. 79 (4) (1996) 938–944.
[18] R. Sakidja, J.H. Perepezko, S. Kim, N. Sekido, Phase stability and structural defects in high-temperature Mo–Si–B alloys, Acta Mater. 56 (18) (2008) 5223–5244.
[19] D. Schliephake, M. Azim, K. von Klinski-Wetzel, B. Gorr, H.-J. Christ, H. Bei, E.P. George, M. Heilmaier, High-temperature creep and oxidation behavior of Mo-Si-B alloys with high Ti contents, Metall. Mater. Trans. A 45 (3) (2014) 1102–1111.
[20] M. Azimovna Azim, S. Burk, B. Gorr, H.-J. Christ, D. Schliephake, M. Heilmaier, R. Bornemann, P.H. Bolívar, Effect of Ti (macro-) alloying on the high-temperature oxidation behavior of ternary Mo–Si–B Alloys at 820–1300 °C, Oxid. Met. 80 (3) (2013) 231–242.
[21] D. Schliephake, C. Gombola, A. Kauffmann, M. Heilmaier, J.H. Perepezko, Enhanced oxidation resistance of Mo–Si–B–Ti alloys by pack cementation, Oxid. Met. 88 (3) (2017) 267–277.
[22] P.K. Ray, Y.Y. Ye, M. Akinc, M.J. Kramer, Effect of Nb and W substitutions on the stability of the A15 Mo3Si phase, J. Alloys Compd. 537 (2012) 65–70.
[23] T. Karahan, G. Ouyang, P.K. Ray, M.J. Kramer, M. Akinc, Oxidation mechanism of W substituted Mo-Si-B alloys, Intermetallics 87 (2017) 38–44.
[24] A. Lange, M. Heilmaier, T.A. Sossamann, J.H. Perepezko, Oxidation behavior of pack-cemented Si–B oxidation protection coatings for Mo–Si–B alloys at 1300 °C, Surf. Coat. Technol. 266 (2015) 57–63.
[25] K. Yanagihara, T. Maruyania, K. Nagata, Dip-coating of Mo(Si, Al)$_2$ on Mo with an Al-Si Melt, Tetsu-to-Hagane 80 (2) (1994) 178–182.
[26] J.S. Park, J.M. Kim, S.H. Cho, Y.I. Son, D. Kim, Oxidation of $MoSi_2$-coated and uncoated TZM (Mo-0.5Ti-0.1Zr-0.02C) Alloys under high temperature plasma flame, Mater. Trans. 54 (8) (2013) 1517–1523.
[27] B. Paul, S. Majumdar, A.K. Suri, Microstructure and mechanical properties of hot pressed Mo-Cr-Si-Ti in-situ composite, and oxidation behavior with silicide coatings, Int. J. Refract. Met. H 38 (2013) 26–34.
[28] K. Ito, T. Murakami, K. Adachi, M. Yamaguchi, Oxidation behavior of Mo-9Si-18B alloy pack-cemented in a Si-base pack mixture, Intermetallics 11 (8) (2003) 763–772.
[29] X.D. Tian, X.P. Guo, Z.P. Sun, Z.Q. Yin, L.J. Wang, Formation of B-modified $MoSi_2$ coating on pure Mo prepared through HAPC process, Int. J. Refract. Met. H 45 (2014) 8–14.
[30] A. Lange, R. Braun, M. Heilmaier, Oxidation behavior of magnetron sputtered double layer coatings containing molybdenum, silicon and boron, Intermetallics 48 (2014) 19–27.
[31] K. Ito, T. Hayashi, M. Yokobayashi, H. Numakura, Evolution kinetics and microstructure of MoSi2 and Mo5Si3 surface layers on two-phase Mo-9Si-18B alloy during pack-cementation and high-temperature oxidation, Intermetallics 12 (4) (2004) 407–415.
[32] S. Majumdar, I.G. Sharma, Oxidation behavior of MoSi2 and Mo(Si, Al)(2) coated Mo-0.5Ti-0.1Zr-0.02C alloy, Intermetallics 19 (4) (2011) 541–545.
[33] N. Nomura, T. Suzuki, K. Yoshimi, S. Hanada, Microstructure and oxidation resistance of a plasma sprayed Mo-Si-B multiphase alloy coating, Intermetallics 11 (7) (2003) 735–742.
[34] S.P. Chakraborty, S. Banerjee, K. Singh, I.G. Sharma, A.K. Grover, A.K. Suri, Studies on the development of protective coating on TZM alloy and its subsequent characterization, J. Mater. Process. Technol. 207 (1–3) (2008) 240–247.
[35] S.P. Chakraborty, S. Banerjee, I.G. Sharma, A.K. Suri, Development of silicide coating over molybdenum based refractory alloy and its characterization, J. Nucl. Mater. 403 (1–3) (2010) 152–159.
[36] S. Majumdar, Formation of MoSi2 and Al doped MoSi2 coatings on molybdenum base TZM (Mo-0.5Ti-0.1Zr-0.02C) alloy, Surf. Coat. Technol. 206 (15) (2012) 3393–3398.
[37] K. Ito, T. Hayashi, M. Yokobayashi, T. Murakami, H. Numakura, Oxidation protective silicide coating on Mo-Si-B alloys, Metall. Mater. Trans. A 36A (3) (2005) 627–636.
[38] H.P. Martinz, B. Nigg, J. Matej, M. Sulik, H. Larcher, A. Hoffmann, Properties of the SIBOR (R) oxidation protective coating on refractory metal alloys, Int. J. Refract. Met. H 24 (4) (2006) 283–291.
[39] O. Senkov, D. Miracle, Effect of the atomic size distribution on glass forming ability of amorphous metallic alloys, Mater. Res. Bull. 36 (12) (2001) 2183–2198.
[40] A.R. Miedema, A.K. Niessen, The enthalpy of solution for solid binary alloys of two 4d-transition metals, Calphad 7 (1) (1983) 27–36.
[41] A.K. Niessen, F.R. de Boer, R. Boom, P.F. de Châtel, W.C.M. Mattens, A.R. Miedema, Model predictions for the enthalpy of formation of transition metal alloys II, Calphad 7 (1) (1983) 51–70.
[42] F.R. De Boer, R. Boom, W.C.M. Mattens, A.R. Miedema, A.K. Niessen, Cohesion in Metals, North Holland, Amsterdam, 1988.
[43] E.S. Domalski, G.T. Armstrong, Heats of Formation of Metallic Borides by Fluorine Bomb Calorimetry, Wright-Patterson Air Force Base, 1964.
[44] Q. Li, D. Zhou, W. Zheng, Y. Ma, C. Chen, Global Structural optimization of tungsten borides, Phys. Rev. Lett. 110 (13) (2013) 136403.
[45] A.K. McMahan, J.E. Klepeis, M. van Schilfgaarde, M. Methfessel, Bonding in the molybdenum silicides, Phys. Rev. B 50 (15) (1994) 10742–10760.
[46] O.J. Lu-Steffes, R. Sakidja, J. Bero, J.H. Perepezko, Multicomponent coating for enhanced oxidation resistance of tungsten, Surf. Coat. Technol. 207 (2012) 614–619.
[47] P.C. Tortorici, M.A. Dayananda, Interdiffusion and diffusion structure development in selected refractory metal silicides, Mater. Sci. Eng., A 261 (1–2) (1999) 64–77.
[48] J.-K. Yoon, K.-W. Lee, S.-J. Chung, I.-J. Shon, J.-M. Doh, G.-H. Kim, Growth kinetics and oxidation behavior of WSi2 coating formed by chemical vapor deposition of Si on W substrate, J. Alloys Compd. 420 (1–2) (2006) 199–206.
[49] J.H. Perepezko, R. Sakidja, Oxidation-resistant coatings for ultra-high-temperature refractory Mo-based alloys, Jom-Us 62 (10) (2010) 13–19.
[50] C.L. Fu, X.D. Wang, Thermal expansion coefficients of Mo-Si compounds by first-principles calculations, Phil. Mag. Lett. 80 (10) (2000) 683–690.